



Virtual Trajectory Augmented Landing Control Based on Dual Quaternion for Lunar Lander

Jae-Wook Kwon*

Korea Advanced Institute of Science and Technology, Daejeon 34133, Republic of Korea

Donghun Lee†

Korea Aerospace Research Institute, Daejeon 34141, Republic of Korea

and

Hyohoong Bang‡

Korea Advanced Institute of Science and Technology, Daejeon 305-701, Republic of Korea

DOI: 10.2514/1.G001459

A pinpoint soft landing with a low touchdown velocity is critical for a lunar lander in the terminal landing phase, particularly with respect to scientific exploration missions. However, the main descent thruster of the lander is usually equipped on one side along the body axis, whereas reaction thrusters for attitude control are fixed in three axes. This causes the translational dynamics and the rotational dynamics of the lunar lander to be mutually coupled. In this study, a new force-torque sequential control law is introduced to resolve the coupling effect. To further improve the coupled motion, a virtual landing trajectory augmented control law is designed. The virtual trajectory is represented as a virtual quaternion and is augmented as a command to the lander's position update using the dual quaternion. A combined augmented landing control algorithm is newly proposed to incorporate the virtual trajectory commands into the force-torque sequential control law. Numerical simulation results with some cases by the Monte Carlo method show that the designed augmented control system enables a terminal soft landing with less fuel consumption.

Nomenclature

F	=	descent thrust force vector of lunar lander (3×1), N
M	=	torque vector of lunar lander (3×1), $\text{N} \cdot \text{m}$
n	=	eigenaxis of rotation (3×1)
p	=	position vector (3×1), m
q	=	quaternion (4×1)
\hat{q}	=	dual quaternion (8×1)
\tilde{q}	=	dual part of dual quaternion (4×1)
r	=	distance vector between current position of lunar lander and target position (3×1), m
u	=	control command vector (3×1)
v	=	velocity vector of lunar lander (3×1), m/s
ϵ	=	dual operator
θ	=	rotation angle for the descent path by the virtual quaternion (1×1), rad
ρ	=	desired angle of departure or arrival, rad
ω	=	angular velocity vector (3×1), rad/s

Subscripts

b	=	body frame
f	=	force vector
i	=	initial
o	=	inertial frame

Received 10 May 2015; revision received 21 January 2016; accepted for publication 15 February 2016; published online 5 July 2016. Copyright © 2016 by the American Institute of Aeronautics and Astronautics, Inc. All rights reserved. Copies of this paper may be made for personal and internal use, on condition that the copier pay the per-copy fee to the Copyright Clearance Center (CCC). All requests for copying and permission to reprint should be submitted to CCC at www.copyright.com; employ the ISSN 0731-5090 (print) or 1533-3884 (online) to initiate your request.

*Ph.D. Candidate, Division of Aerospace Engineering, 335, Gwahangno, Yuseong; currently Senior Researcher, Division of Lunar Exploration Research, Korea Aerospace Research Institute, Gwahangno, Yuseong, Daejeon 34133, Republic of Korea.

†Senior Researcher, Division of Lunar Exploration Research, 115 Gwahangno, Yuseong.

‡Professor, Department of Aerospace Engineering, 335 Gwahangno, Yuseong.

t	=	target
τ	=	torque vector

Superscripts

r	=	real value with respect to lander
v	=	virtual value with respect to descent path

I. Introduction

THE primary focus of this paper is to design a lunar landing control that enables pinpoint target accuracy and terminal vertical descending. With respect to the landing algorithm, the designed algorithm from the Apollo landing mission has been widely used in recent planetary landing missions. Because the Apollo landing procedure is divided into three phases after the deorbit burn [1–3], three subphases in the powered descent phase that are crucial for a safe soft lunar landing can be summarized and distinguished. Significant research efforts have been dedicated to studying the guidance and control techniques for the three phases of lunar landing [1–19].

When taking into account the landing conditions of future lunar missions, such as pinpoint landing accuracy within 10 m of the target site [11,20], two points for lunar missions should be carefully considered: achieving a soft landing and a pinpoint landing during the terminal landing phase. An analytical targeting real-time guidance algorithm has been presented that allows for the separate use of a targeting and real-time guidance algorithm to generate trajectories before descent initiation based on analytical solutions to the equations for speed, downrange, altitude, and time as a function of the flight-path angle as well as assume arcs of thrust acceleration [21]. A powered-descent guidance algorithm to generate the minimum-landing-error trajectory (the trajectory that minimizes the distance to the prescribed target while using the available fuel using an optimization approach) was implemented. Recently, because the flight onboard computer enables processing of massive data, the state-of-the-art work in real-time optimal powered landing trajectory design has been introduced to achieve minimum-landing-error capability under limited fuel and the minimum-fuel trajectory to the target [20,22].

A number of studies have been conducted on soft landing processes [8–11]. Two phases of the soft landing process have been considered: 1) the powered descent phase into a low velocity for

descent to the vicinity of the target position (about several kilometers), during which the lander is greatly decelerated but consumes a large amount of fuel; and 2) the terminal landing phase, during which the lunar lander softly lands on the preselected site with a vertical attitude. In the most recent research, during the terminal landing phase, a gravity-turn guidance law has been considered [10,12]. This law aims to simultaneously assure the position and the attitude of the lunar lander to satisfy landing requirements at the moment of touchdown. As such, the position and attitude of a lunar lander shall be considered to simultaneously meet the requirements during descent of the lunar lander because the required thrust vector depends on the attitude maneuvering. Gravity-turn guidance laws relevant to a lunar lander, while in the descent phase, have been extensively studied for many years with the configuration of the main thruster aligned with the opposite velocity vector [13–18]. If the attitude of the lunar lander is made to vertically align with the gravity of the moon, at terminal touchdown with fuel consumption minimized, it can be expressed in a planar framework. However, in practical terms in three degrees of freedom (DOFs), it is not easy to develop a soft landing scenario. Moreover, an important consideration is equipping the main descent thruster, which controls the position, on one side, generating thrust along one axis in the body frame, and reaction thrusters, which control the attitude and provide maneuverability in three axes. This requires a control law to resolve the problem of the dynamic coupling effect. One of the reasons for this is that the translational dynamics and the rotational dynamics of the lunar lander are mutually coupled in six DOFs. As such, this is one of the design considerations for a soft landing with a vertical body direction.

It is therefore necessary to carefully consider crucial points for lunar missions: achieving a pinpoint soft landing with less fuel consumption. In this study, we design a control algorithm to attain these objectives by resolving the formulated dynamic coupling problem mentioned previously. The proposed landing control algorithm consists of three controllers: 1) a virtual trajectory controller, 2) a lander position controller, and 3) a lander attitude controller. First, the virtual trajectory controller updates the descent-path angle as a virtual quaternion that we augment to the lander's position as a direction command. This augmentation is handled by the dual quaternion formula. The designed virtual trajectory generated by the virtual trajectory controller was augmented as a direction command with partial guidance. The virtual trajectory controller is expected to meet the requirement for a soft landing with a vertical direction landing at the touchdown moment. Moreover, we introduce a force-torque sequential control law, as we connect a lander position controller and a lander attitude controller. The point of connection is the vector information between the force command and the attitude command. Control torque is generated with the attitude error computed by the attitude command, which should align the lander's attitude vector with the vector of the lander's thruster firing for position control. This sequential control law can resolve the coupled dynamic effect and align the lander's body axis on the axis of the target position. The soft landing requirement can be met with the proposed controllers. Additionally, a pinpoint soft landing is ensured by the dual quaternion, wherein we use the position error with the virtual trajectory command in the lander position controller. The proposed lunar landing control system that is introduced in this paper as a virtual trajectory augmented lunar landing control system is sequentially combined with the preceding three controllers.

Dual quaternions provide a compact, unambiguous, singularity-free, and computational minimalistic rigid transformation because they offer a unified framework for the translation and rotation into a single state variable. Clifford [23] first introduced dual numbers, and their application to rigid-body kinematics was subsequently generalized by Yang and Freudenstein [24]. The dual quaternion is mostly used for kinematic analyses [25–33]. In the field of spacecraft control, research papers based on the dual quaternion have been released [26–28]. However, the most widely proposed approach is to use a logarithm controller by the characteristics of the dual quaternion and to handle state variables represented by a dual quaternion form to combine the translation and rotation states in the control loop [27,28].

Herein, we use the dual quaternion in a different manner from that introduced in other papers. The main function of the dual quaternion in this research is to improve the descent-path angle by the update of the virtual attitude. We attempt to augment the lander's descent-path direction command to the lander's position for a pinpoint landing based on the kinematics of dual quaternions.

The remaining part of this paper is organized as follows. The mathematical preliminaries of dual quaternions are introduced in Sec. II. The lander's position update with the augmented trajectory command is described in Sec. III. In Sec. IV, the translational and rotational coupled dynamic model of a lunar lander with a single descent thruster aligned with the lander's body axis is introduced. Finally, to deal with the coupled dynamic model, a designed force-torque sequential control law is introduced, allowing the lander to descend with a vertical attitude. The sequential controller is then integrated to the virtual controller under the dual quaternion formula with multiplication of the virtual trajectory command and the lander's position, which is discussed in Sec. V. In Sec. VI, numerical simulation results by the Monte Carlo method are presented, demonstrating that a lunar lander can be controlled to descend at the desired target position and retargeted landing site with a vertical landing direction for a safe soft landing in several cases.

II. Mathematical Preliminaries

This section explains the dual quaternion and its kinematics used to construct the descent path on the landing control process. First, the explanation of the quaternion is presented, followed by a short description of the Plücker coordinates. The dual quaternion and its relevant properties are then introduced. More details on these subjects can be found in the pertinent literature [34–37].

A. Quaternions

The quaternion is defined as a vector, an extension of complex numbers to a four-dimensional manifold. There are two formalisms to define a quaternion [36]. The definition of a quaternion is a pair $\mathbf{q} = (\mathbf{q}_v, q_s)$, where $\mathbf{q}_v \in \mathbb{R}^{3 \times 1}$ and $q_s \in \mathbb{R}$. By definition, a quaternion satisfies the following arithmetic operations:

$$\begin{aligned}\lambda(\mathbf{q}_v, q_s) &= (\lambda\mathbf{q}_v, \lambda q_s) \\ \mathbf{q}_1 + \mathbf{q}_2 &= (\mathbf{q}_{v1} + \mathbf{q}_{v2}, q_{s1} + q_{s2}) \\ \mathbf{q}_1 \circ \mathbf{q}_2 &= (q_{s1}\mathbf{q}_{v2} + q_{s2}\mathbf{q}_{v1} + \mathbf{q}_{v1} \times \mathbf{q}_{v2}, q_{s1}q_{s2} - \mathbf{q}_{v1}\mathbf{q}_{v2}) \\ \|\mathbf{q}\| &= \mathbf{q} \circ \mathbf{q}^*\end{aligned}\quad (1)$$

If $\|\mathbf{q}\| = 1$, $\mathbf{q} \in \mathbb{R}^{4 \times 1}$ and is a unit quaternion. The unit quaternion can be used to represent a rotation of an angle θ about a unit vector $\mathbf{n} \in \mathbb{R}^{3 \times 1}$ in the three-dimensional Euclidean space as previously reported:

$$\mathbf{q} = \left[\sin\left(\frac{\theta}{2}\right)\mathbf{n}, \cos\left(\frac{\theta}{2}\right) \right]^T \quad (2)$$

B. Dual Quaternions

This section briefly outlines the dual quaternions. A dual quaternion is a widely used quaternion with dual number components $\hat{\mathbf{q}} = [\hat{\mathbf{q}}_v, \hat{q}_s]$, where $\hat{\mathbf{q}}_v$ is a dual vector, whereas \hat{q}_s is a dual scalar part. A dual quaternion can also be defined as [38,39]

$$\hat{\mathbf{q}} = \mathbf{q} + \varepsilon \tilde{\mathbf{q}} \quad (3)$$

where \mathbf{q} and $\tilde{\mathbf{q}}$ are both quaternions. The quaternions \mathbf{q} and $\tilde{\mathbf{q}}$ are called the “real part” and the “dual part” of the dual quaternion, respectively. Dual vector quaternions and dual scalar quaternions are dual quaternions formed for vector quaternions and scalar quaternions, respectively. Alternatively, the dual quaternions can be mapped in a vector space as follows:

$$\hat{\mathbf{q}} = [q_1, q_2, q_3, q_4, q_5, q_6, q_7, q_8]^T \quad (4)$$

Let $\mathbf{q} \in \mathbb{R}^{4 \times 1}$ and $\mathbf{p} \in \mathbb{R}^{3 \times 1}$ be a unit quaternion for an attitude representation and position vector. \mathbf{q} is defined with a normalized Euler-axis vector $\mathbf{n} \in \mathbb{R}^{3 \times 1}$ and a rotational angle θ around the Euler axis. Similar to Eq. (2), the dual quaternion can be defined as a rotational angle $\hat{\theta}$ about the Euler axis $\hat{\mathbf{n}}$ as

$$\hat{\mathbf{q}} = \left[\sin\left(\frac{\hat{\theta}}{2}\right)\hat{\mathbf{n}}, \cos\left(\frac{\hat{\theta}}{2}\right) \right]^T \quad (5)$$

A quaternion $\tilde{\mathbf{q}} \in \mathbb{R}^{4 \times 1}$ for a position representation from Eqs. (3) and (5) is defined as

$$\tilde{\mathbf{q}} = \frac{1}{2} \begin{bmatrix} \mathbf{p}_o \\ 0 \end{bmatrix} \circ \mathbf{q} \quad (6)$$

$$\tilde{\mathbf{q}} = \frac{1}{2} \mathbf{q} \circ \begin{bmatrix} \mathbf{p}_b \\ 0 \end{bmatrix} \quad (7)$$

where $\mathbf{p}_o \in \mathbb{R}^{3 \times 1}$ and $\mathbf{p}_b \in \mathbb{R}^{3 \times 1}$ are position vectors in the inertial and body frames, respectively.

The elementary arithmetic operations necessary for the dual quaternions are

$$\begin{aligned} \lambda\hat{\mathbf{q}} &= \lambda\mathbf{q} + \varepsilon\lambda\tilde{\mathbf{q}} \\ \hat{\mathbf{q}}_1 + \hat{\mathbf{q}}_2 &= \mathbf{q}_1 + \mathbf{q}_2 + \varepsilon(\tilde{\mathbf{q}}_1 + \tilde{\mathbf{q}}_2) \\ \hat{\mathbf{q}}_1 \circ \hat{\mathbf{q}}_2 &= (\mathbf{q}_1 + \varepsilon\tilde{\mathbf{q}}_1) \circ (\mathbf{q}_2 + \varepsilon\tilde{\mathbf{q}}_2) \\ &= \mathbf{q}_1 \circ \mathbf{q}_2 + \varepsilon(\mathbf{q}_1 \circ \tilde{\mathbf{q}}_2 + \tilde{\mathbf{q}}_1 \circ \mathbf{q}_2) \\ \hat{\mathbf{q}}^* &= (\mathbf{q} + \varepsilon\tilde{\mathbf{q}})^* = \mathbf{q}^* + \varepsilon\tilde{\mathbf{q}}^* = -\mathbf{q} - \varepsilon\tilde{\mathbf{q}} \end{aligned} \quad (8)$$

where \mathbf{q}^* and $\tilde{\mathbf{q}}^*$ are conjugations of the corresponding quaternion \mathbf{q} and $\tilde{\mathbf{q}}$, respectively.

III. Trajectory Command

A. Lunar Landing Coordinate System

Before the introduction of the new algorithm proposed in this paper, we first define a coordinate system for the lunar landing for understanding the displacement by the dual quaternion. As shown in Fig. 1, let $O - X_o Y_o Z_o$ be an inertial frame. The lunar lander is considered as a rigid body; meanwhile, a body frame $B - x_b y_b z_b$ is

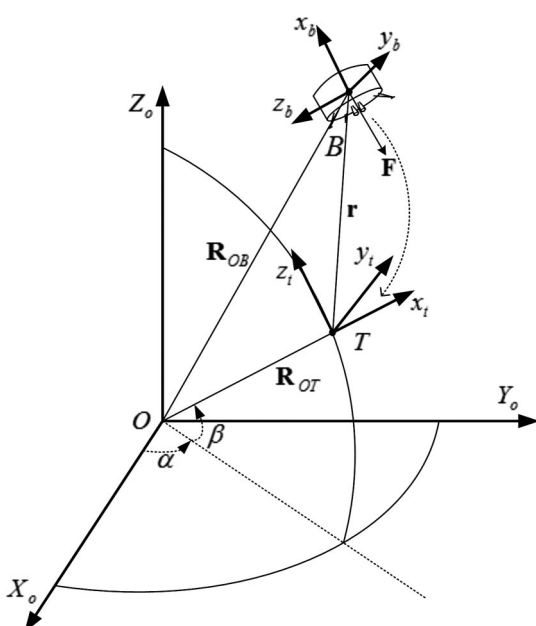


Fig. 1 Lunar landing coordinate system in terminal descent phase.

defined with the origin at the center of mass. The subscript o indicates an inertial frame, whereas the subscript b indicates the rotating body frame. The subscript t expresses the desired target frame.

B. Set of Desired Departure and Arrival Angles

To obtain the desired descent-path angles of departure and arrival by dual quaternions on the Plücker coordinates, we propose the following procedure.

Departure angle: The procedure for generating the desired descent-path angle at the departure point is to set the departure angle ρ_i by using the Euler angle rotation approach as given in Eq. (9):

$$\boldsymbol{\rho}_i = [\rho_{x_i} \quad \rho_{y_i} \quad \rho_{z_i}]^T \quad (9)$$

The set of departure angle with respect to the x_t , y_t , and z_t axes in the target frame is described in Fig. 5. To acquire a quaternion form, the direction cosine matrix (DCM) $[A(\boldsymbol{\rho}_i)]$ is taken as to the individual angular rotations about the target frame.

The quaternion \mathbf{q}_i with the information of the departure angle is obtained as Eqs. (10–12):

$$\mathbf{C}_{3 \times 3} = [A(\boldsymbol{\rho}_i)] = [A(\rho_{x_i})][A(\rho_{y_i})][A(\rho_{z_i})] \quad (10)$$

Furthermore,

$$\begin{aligned} q_{4i} &= \pm \frac{1}{2} \sqrt{1 + c_{11} + c_{22} + c_{33}} \\ q_{1i} &= (c_{23} - c_{32})/4q_{4i} \\ q_{2i} &= (c_{31} - c_{13})/4q_{4i} \\ q_{3i} &= (c_{12} - c_{21})/4q_{4i} \end{aligned} \quad (11)$$

so that

$$\mathbf{q}_i = [q_{1i} \quad q_{2i} \quad q_{3i} \quad q_{4i}]^T \quad (12)$$

Descending angle: For descending with a vertical landing, ρ_t is set as $[0 \quad 0 \quad 0]^T$ so that the terminal descent path will be aligned on the x_t axis on the target frame $T - x_t y_t z_t$. The procedure to acquire the descent-path angle is the same as that defined in Eqs. (10–12).

C. Position Update with the Augmented Trajectory Command

The quaternion \mathbf{q} obtained from Eqs. (10–12) has information for the trajectory. We use the quaternion \mathbf{q} to build a dual quaternion $\hat{\mathbf{q}}$. The dual part $\tilde{\mathbf{q}}$ of the dual quaternion $\hat{\mathbf{q}}$ has the position information. We use the dual part $\tilde{\mathbf{q}}$ at the later position update step. The dual quaternion notation is given in Eq. (13) with the position information in $\tilde{\mathbf{q}}$:

$$\hat{\mathbf{q}} = \mathbf{q} + \varepsilon\tilde{\mathbf{q}} \quad (13)$$

$$\tilde{\mathbf{q}} = \frac{1}{2} \begin{bmatrix} \mathbf{p}_o \\ 0 \end{bmatrix} \circ \mathbf{q} \quad (14)$$

Herein, we use a unit quaternion \mathbf{q} as a virtual quaternion to generate the lander's trajectory. Therefore, the unit quaternion \mathbf{q} is named a virtual quaternion \mathbf{q}^v with the superscript v , which indicates the virtual status for generating a descent path for kinematics not used for real dynamics. To clearly define the virtual status and the real status, some variables with the superscript r are used for the real status, which will be used to represent real dynamics such as the real position \mathbf{p}' of moving objects. We represent the initial and target quaternion \mathbf{q}_i and \mathbf{q}_t as \mathbf{q}_i^v and \mathbf{q}_t^v for the virtual quaternion, which are newly renamed because they are used not to control the real dynamics and kinematics but to construct the descent path through position control. The virtual dual quaternion $\hat{\mathbf{q}}^v$ is defined with the virtual quaternion \mathbf{q}^v for the changed descent-path angles and the multiplication of \mathbf{q}^v and the real current position \mathbf{p}' of the moving object on the trajectory:

$$\hat{\mathbf{q}}^v = \mathbf{q}^v + \epsilon \tilde{\mathbf{q}}^v = \mathbf{q}^v + \epsilon \frac{1}{2} \mathbf{p}^r \circ \mathbf{q}^v \quad (15)$$

$$\tilde{\mathbf{q}}^v = \frac{1}{2} \mathbf{p}^r \circ \mathbf{q}^v \quad (16)$$

The new algorithm is now introduced to generate descent paths of a lunar lander based on the proposed virtual dual quaternion approach. In addition, the path angle of the target point is perpendicular to the x_t axis and $y_t z_t$ plane. A descent path is constructed with position control only by applying the dual quaternion when two different positions, which correspond to the initial and target positions, are given.

IV. Lunar Lander Dynamics

In this section, the lunar landing dynamics problem is analyzed with a desired position and attitude in the powered descending phase. An important issue that should be considered is the coupling effect between translational and rotational motion. Specifically, because the lunar module is equipped with a main thruster only providing thrust along one axis of the body frame and attitude control actuators providing maneuverability in three axes, the thrust orientation for orbit control only depends on the lander's attitude and the thruster installation matrix. This implies that the translational dynamics and the attitude dynamics are mutually coupled and should be taken into account simultaneously. The principal coordinate system is a spherical coordinate system, and the moon is modeled as a spherical body of uniform gravity with no atmosphere and no gravitational harmonics [40].

A. Moon-Centered Inertial Frame

For translational dynamics modeling, we use a moon-centered inertial frame, as shown in Fig. 1. $O - X_o Y_o Z_o$ of the inertial frame is based at the center of the moon. The $X_o Y_o$ plane coincides with the moon equatorial plane; the points on the X_o axis are 0° longitude, and the target point T represents the latitude of the lunar surface. Then, the target coordinate frame x_t is the axis pointing toward outer space on \mathbf{R}_{OT} from the origin, and the z_t axis is pointing north, Z_o . The y_t axis of the target point T is perpendicular to the lunar surface. Furthermore, the body frame is formulated in an identical manner to the target frame when the lunar lander lands at the T point. The main thruster used for descent landing is aligned with the $-x_b$ axis, and its force is expressed as \mathbf{v} . \mathbf{R}_{OB} represents the distance between the lander and the center of the moon. \mathbf{R}_{OT} and \mathbf{r} denote the distances from O to T and T to B , respectively [40].

The position vector between the target and the lunar lander is defined as follows:

$$\mathbf{r} = \mathbf{R}_{OB} - \mathbf{R}_{OT} \quad (17)$$

The target position \mathbf{p}_t can be written as

$$\mathbf{R}_{OT} = \mathbf{p}_t = [p_{tx}, p_{ty}, p_{tz}] \quad (18)$$

where

$$\begin{aligned} p_{tx} &= R_{OT} \cos \beta \cos \alpha \\ p_{ty} &= R_{OT} \cos \beta \sin \alpha \\ p_{tz} &= R_{OT} \sin \beta \end{aligned} \quad (19)$$

B. Quaternion and Direction Cosine Matrix

The body frame of the lunar lander is defined with the origin at the center of mass, and unit vectors coincide with their principal axes of inertia. For the rotational relationship, the attitude transformation matrix from the target frame T to the body frame B can be derived as quaternions in terms of the DCM:

$$\begin{aligned} [\mathbf{A}(\mathbf{q})] \\ = \begin{bmatrix} q_1^2 - q_2^2 - q_3^2 + q_4^2 & 2(q_1 q_2 + q_3 q_4) & 2(q_1 q_3 - q_2 q_4) \\ 2(q_1 q_2 - q_3 q_4) & -q_1^2 + q_2^2 - q_3^2 + q_4^2 & 2(q_2 q_3 + q_1 q_4) \\ 2(q_1 q_3 + q_2 q_4) & 2(q_2 q_3 - q_1 q_4) & -q_1^2 - q_2^2 + q_3^2 + q_4^2 \end{bmatrix} \end{aligned} \quad (20)$$

C. Orbital and Attitude Coupled Dynamics

As in Fig. 1, the lunar lander considered herein is equipped with a main descent thruster aligned with the $-x_b$ axis and reaction thrusters for producing control torques in three axes. The thrust vector \mathbf{F} is aligned with the x_b direction of the body frame, $\mathbf{F} = [F \ 0 \ 0]^T$. Therefore, the dependence of the thrust orientation for translational control of the lunar lander rotation is coupled [38,39]. To obtain the force vector under consideration with respect to the thrust vector with the x_b axis only, the control force of Eq. (21) is multiplied with DCM of Eq. (20) and the thrust vector:

$$\mathbf{F} = \|\mathbf{u}_f\|[\mathbf{A}(\mathbf{q})]^T[1 \ 0 \ 0]^T \quad (21)$$

The motions of the lunar lander can be described as

$$\ddot{\mathbf{R}}_{OB} = -\frac{\mu}{\|\mathbf{R}_{OT} + \mathbf{r}\|^3} \mathbf{R}_{OB} + \frac{\mathbf{F}}{m} \quad (22)$$

where μ denotes the moon's gravitational parameter, and m represents the mass of the module. In the target frame, let $\mathbf{F} = [F_x, F_y, F_z]^T \in \mathbb{R}^3$, and $\mathbf{r} = [x, y, z]^T \in \mathbb{R}^3$, whereas the attitude dynamics of the lunar lander is governed by

$$\begin{aligned} \mathbf{M} &= \dot{\mathbf{h}}_o = \dot{\mathbf{h}}_b + \boldsymbol{\omega} \times \mathbf{h} \\ &= \mathbf{I} \dot{\boldsymbol{\omega}} + \boldsymbol{\omega} \times \mathbf{I} \boldsymbol{\omega} \end{aligned} \quad (23)$$

where the angular momentum vector is \mathbf{h} ; the subscript o indicates a derivative in the inertial frame, and the subscript b indicates a derivative in the rotating body frame. Therefore, Eqs. (22) and (23) constitute the orbital and attitude dynamics of the lunar lander. The term $\boldsymbol{\omega} = [\omega_1 \ \omega_2 \ \omega_3]^T$ is the angular velocity vector about the body coordinate axes.

The differential equations of the quaternion kinematics are readily available as

$$\begin{bmatrix} \dot{q}_1 \\ \dot{q}_2 \\ \dot{q}_3 \\ \dot{q}_4 \end{bmatrix} = \frac{1}{2} \begin{bmatrix} q_2 \omega_3 - q_3 \omega_2 + q_4 \omega_1 \\ -q_1 \omega_3 + q_3 \omega_1 + q_4 \omega_2 \\ q_1 \omega_2 - q_2 \omega_1 + q_4 \omega_3 \\ -q_1 \omega_1 - q_2 \omega_2 - q_3 \omega_3 \end{bmatrix} \quad (24)$$

In order for the preceding translational and rotational dynamics to be simultaneously controlled, an integrated controller of modern control techniques such as a robust controller may be considered. However, we propose a new concept by taking advantage of a conventional proportional-derivative (PD) control approach to resolve the coupled dynamics problem. In the next section, the modified controller is proposed.

V. Landing Controller Design

In this section, we discuss the following three newly proposed controllers: 1) virtual trajectory controller, 2) landing position controller, and 3) lander attitude controller.

To reiterate, the dual quaternion notation is defined in Eq. (3) as $\hat{\mathbf{q}} = \mathbf{q} + \epsilon \tilde{\mathbf{q}}$:

$$\mathbf{X} = [\hat{\boldsymbol{\omega}} \ \hat{\mathbf{q}} \ \boldsymbol{\omega}^r \ \mathbf{q}^r] \quad (25)$$

where

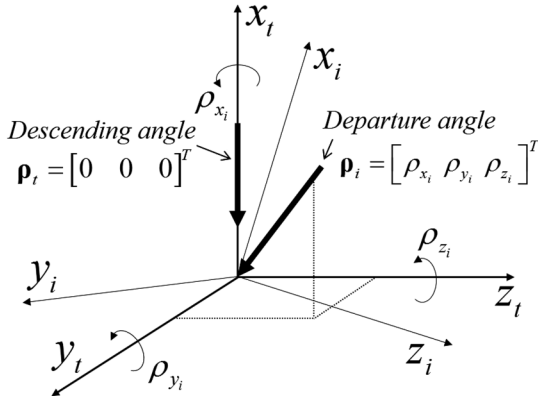


Fig. 2 Departure and descending angles represented by angular rotations.

$$\hat{q} = q^v + \varepsilon \tilde{q}^v = q^v + \varepsilon \frac{1}{2} \mathbf{p}^r \circ \mathbf{q}^v \quad (26)$$

$$\hat{\omega} = \omega^v + \varepsilon v^v \quad (27)$$

The proposed landing controller using the dual quaternion has state variables as given in Eq. (30). The superscripts v and r of Eqs. (25–27) are the same as those expressed in Eqs. (15) and (16). The procedure for constructing the descent path with the proposed algorithm based on the dual quaternion is presented in Eqs. (9–16) and Fig. 2. The necessary control commands are grouped as 1) virtual control torque \mathbf{u}_t^v for the descent-path direction, 2) landing position control force \mathbf{u}_f^r , 3) real quaternion command $\mathbf{q}_{\text{com}}^r$ for the lander attitude, and 4) real attitude control torque \mathbf{u}_t^r , as follows:

$$\mathbf{U} = [\mathbf{u}_t^v \ \mathbf{u}_f^r \ \mathbf{q}_{\text{com}}^r \ \mathbf{u}_t^r]^T \quad (28)$$

A. Lunar Landing Sequential Controller Design

The position control force \mathbf{u}_f^r is designed in the following steps.

The lunar lander dynamics are the same as in the previous section, and the designed control force is originally formulated such that

$$\mathbf{u}_f^r = -\mathbf{K}_{pf}^r(\mathbf{p}^r - \mathbf{p}_{\text{com}}^r) - \mathbf{K}_{df}^r(\mathbf{v}^r - \mathbf{v}_{\text{com}}^r) - \mathbf{F}_g m \quad (29)$$

where $\mathbf{K}_{pf}^r = \text{diag}[K_{pf1}^r, K_{pf2}^r, K_{pf3}^r]$ and $\mathbf{K}_{df}^r = \text{diag}[K_{df1}^r, K_{df2}^r, K_{df3}^r]$ are control gains. Herein, $\mathbf{p}_{\text{com}}^r$ is the target position \mathbf{p}_t^r as command inputs in Eq. (29), and $\mathbf{v}_{\text{com}}^r$ is the target velocity. To control the position while the lunar module is descending, the control force should be mainly considered due to the limited thruster capability aligned with one axis. Fortunately, in this case, the attitude of the lander naturally assumes the desired attitude at the terminal landing phase due to the gravity effect. Therefore, with this background information and the designed controller, an integrated PD controller is constructed by reusing the force vector in the attitude command.

The control force yields the position vector as follows:

$$\mathbf{u}_f^r = \mathbf{u}_f^r / \|\mathbf{u}_f^r\|, \quad u_f^r = [u_{11f}^r \ u_{21f}^r \ u_{31f}^r]^T \quad (30)$$

The Euler angles of the force command vector can be obtained as

$$\phi_{\text{com}}^r = 0 \quad \varphi_{\text{com}}^r = \text{asin}(-u_{31f}^r) \quad \psi_{\text{com}}^r = \text{atan2}(u_{21f}^r, u_{11f}^r) \quad (31)$$

Equation (31) is delivered from the transformation matrix Eq. (32) from the target frame to the body frame:

$$[\mathbf{A}(\Theta)] = R_{x_b}(\phi) \cdot R_{y_b}(\varphi) \cdot R_{z_b}(\psi)$$

$$= \begin{bmatrix} c\varphi c\psi & c\varphi s\psi & -s\varphi \\ -c\varphi s\psi + s\varphi s\phi c\psi & c\phi c\psi + s\varphi s\psi s\phi & c\phi s\phi \\ s\varphi s\psi + s\varphi c\phi c\psi & -s\phi c\psi + s\varphi s\psi c\phi & c\phi c\phi \end{bmatrix} \quad (32)$$

where $\Theta = [\phi \ \varphi \ \psi]^T \in \mathfrak{R}^3$, and ϕ , φ , and ψ denote Euler angles revolving about the z_b , y_b , and x_b axes, respectively:

$$\mathbf{F} = \begin{bmatrix} F_x \\ F_y \\ F_z \end{bmatrix} = [\mathbf{A}(\Theta)]^T \begin{bmatrix} F \\ 0 \\ 0 \end{bmatrix} = \begin{bmatrix} F \cos \varphi \cos \psi \\ F \cos \varphi \sin \psi \\ -F \sin \varphi \end{bmatrix} = \begin{bmatrix} u_{11f}^r \\ u_{21f}^r \\ u_{31f}^r \end{bmatrix} \quad (33)$$

The thrust vector \mathbf{F} of Eq. (33) is aligned with the x_b direction of the body frame. The dependence of the thrust orientation for position control on the lander attitude is delineated by Eq. (33). Therefore, the DCM for the attitude commands can be described as Eqs. (34–38):

$$\begin{aligned} [\mathbf{A}_{\phi \text{ com}}^r] &= \begin{bmatrix} 1 & 0 & 0 \\ 0 & c\phi_{\text{com}}^r & s\phi_{\text{com}}^r \\ 0 & -s\phi_{\text{com}}^r & c\phi_{\text{com}}^r \end{bmatrix} \\ [\mathbf{A}_{\varphi \text{ com}}^r] &= \begin{bmatrix} c\varphi_{\text{com}}^r & 0 & -s\varphi_{\text{com}}^r \\ 0 & 1 & 0 \\ s\varphi_{\text{com}}^r & 0 & c\varphi_{\text{com}}^r \end{bmatrix} \\ [\mathbf{A}_{\psi \text{ com}}^r] &= \begin{bmatrix} c\psi_{\text{com}}^r & s\psi_{\text{com}}^r & 0 \\ -s\psi_{\text{com}}^r & c\psi_{\text{com}}^r & 0 \\ 0 & 0 & 1 \end{bmatrix} \end{aligned} \quad (34)$$

and

$$\mathbf{C}_{3 \times 3}^r = [\mathbf{A}_{321}^r] = [\mathbf{A}_{\psi\varphi\phi}^r] = [\mathbf{A}_{\phi \text{ com}}^r][\mathbf{A}_{\varphi \text{ com}}^r][\mathbf{A}_{\psi \text{ com}}^r] \quad (35)$$

Furthermore,

$$\begin{aligned} q_{4 \text{ com}}^r &= \pm \frac{1}{2} \sqrt{1 + c_{11}^r + c_{22}^r + c_{33}^r} \\ q_{1 \text{ com}}^r &= (c_{23}^r - c_{32}^r)/4q_4^r \\ q_{2 \text{ com}}^r &= (c_{31}^r - c_{13}^r)/4q_4^r \\ q_{3 \text{ com}}^r &= (c_{12}^r - c_{21}^r)/4q_4^r \end{aligned} \quad (36)$$

so that

$$\mathbf{q}_{\text{com}}^r = [q_{1 \text{ com}}^r \ q_{2 \text{ com}}^r \ q_{3 \text{ com}}^r \ q_{4 \text{ com}}^r] \quad (37)$$

and

$$\mathbf{q}_e^r = \mathbf{q}_{\text{com}}^{r*} \circ \mathbf{q}^r \quad (38)$$

Representing the attitude of a body in a reference frame by a DCM requires knowledge on nine parameters c_{ij} of Eq. (35), whereas only four q_i ($i = 1, 2, 3, 4$) parameters of Eq. (36) are needed when using the quaternion. Moreover, the other newly proposed control law is designed based on the dual quaternion. Therefore, a quaternion feedback control is employed instead of Euler angle feedback control for convenience and efficient comparison of the progressed same formulas. Quaternion errors are needed for the attitude control, and quaternion commands are obtained from Eqs. (34–38) [41]. The attitude control torque \mathbf{u}_t^r is obtained with the quaternion error \mathbf{q}_e^r derived from the force vector of Eq. (38):

$$\mathbf{u}_t^r = -\mathbf{K}_{pt}^r \mathbf{q}_e^r - \mathbf{K}_{dt}^r \boldsymbol{\omega}_e^r + \boldsymbol{\omega}^r \times \mathbf{I} \boldsymbol{\omega}^r \quad (39)$$

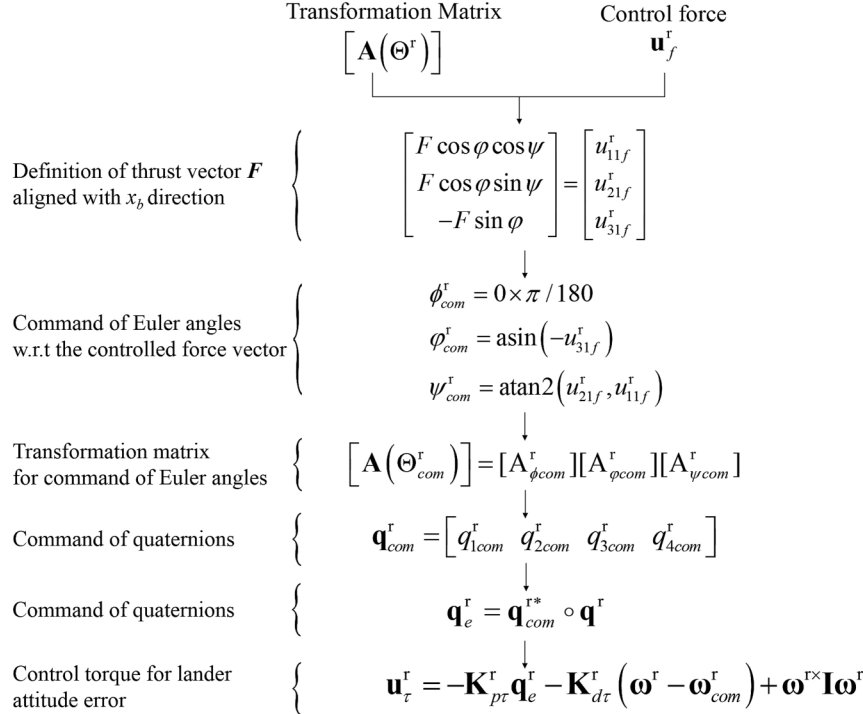


Fig. 3 Control flow of lander attitude error for position vector.

where $\mathbf{K}_{p\tau}^r = \text{diag}[K_{p\tau 1}^r, K_{p\tau 2}^r, K_{p\tau 3}^r]$ and $\mathbf{K}_{d\tau}^r = \text{diag}[K_{d\tau 1}^r, K_{d\tau 2}^r, K_{d\tau 3}^r]$ are control gains. Herein, $\boldsymbol{\omega}_e^r$ is the real angular velocity error as $\boldsymbol{\omega}^r - \boldsymbol{\omega}_{com}^r$, and $\boldsymbol{\omega}_{com}^r$ is the real target angular velocity vector.

B. Virtual Trajectory Controller Design

The lander's trajectory is designed using the kinematics of the dual quaternion, which is described in Sec. III. Therefore, we apply quaternions, which are usually used for the attitude control, into the descent-path angle control. The method to obtain the quaternions for the angles of departure and vertical arrival at the lander's positions \mathbf{p}_t and \mathbf{p}_f (Fig. 4) is described previously. The quaternions \mathbf{q}_t^v and \mathbf{q}_f^v referred in the lander's attitude are then used to construct the descent direction, and the quaternion \mathbf{q}^v is updated by following the control process.

The virtual quaternion error is derived from the virtual quaternion such that

$$\mathbf{q}_e^v = \mathbf{q}_t^{v*} \circ \mathbf{q}^v \quad (40)$$

where \mathbf{q}_e^v is the virtual quaternion error. However, we redefine Eq. (40) as Eq. (41) to substitute the current virtual quaternion \mathbf{q}^v into \mathbf{q}_{com}^r of Eq. (37) to expect variable gain effect of the following position controller \mathbf{u}_f^r :

$$\mathbf{q}_e^v = \mathbf{q}_t^{v*} \circ \mathbf{q}_{com}^r \quad (41)$$

The lander follows the trajectory with the desired descending angles. Therefore, we propose a new concept of position error

by augmenting the preobtained descending angle error \mathbf{q}_e^v of Eq. (41).

First, the virtual dual error quaternion is introduced as Eq. (42):

$$\hat{\mathbf{q}}_e^v = \hat{\mathbf{q}}_t^{v*} \circ \hat{\mathbf{q}}^v, \quad \tilde{\mathbf{q}}_e^v = \mathbf{q}_e^v + \varepsilon \tilde{\mathbf{q}}_e^v \quad (42)$$

The virtual control torque that makes the descent-path angle to converge to the desired arrival angle in the trajectory is designed as

$$\mathbf{u}_\tau^v = -\mathbf{K}_{p\tau}^v \mathbf{q}_e^v - \mathbf{K}_{d\tau}^v \boldsymbol{\omega}_e^v + \boldsymbol{\omega}^v \times \mathbf{I} \boldsymbol{\omega}^v \quad (43)$$

where $\mathbf{K}_{p\tau}^v = \text{diag}[K_{p\tau 1}^v, K_{p\tau 2}^v, K_{p\tau 3}^v]$ and $\mathbf{K}_{d\tau}^v = \text{diag}[K_{d\tau 1}^v, K_{d\tau 2}^v, K_{d\tau 3}^v]$ are control gains.

Herein, $\tilde{\mathbf{q}}_e^v$ is a dual part error combined with the virtual quaternion error \mathbf{q}_e^v of Eq. (42) and the position error between the current position \mathbf{p}^r and the target position \mathbf{p}_f^r of the lunar lander. Second, the control force with the dual part error $\tilde{\mathbf{q}}_e^v$ of the virtual dual error quaternion $\hat{\mathbf{q}}_e^v$ is considered. The main contribution of this study is to use the dual part error $\tilde{\mathbf{q}}_e^v$ as the lander's position error obtained from $\tilde{\mathbf{q}}_e^v = \frac{1}{2} \mathbf{p}_e^r \circ \mathbf{q}_e^v$ with the real quaternion command \mathbf{q}_{com}^r of Eq. (42). Therefore, the descent direction with the path-angle at the current position can be constructed. The new control force is constructed as

$$\mathbf{u}_f^r = -[\mathbf{A}(\mathbf{q}^v)]^T \mathbf{K}_{p\tau} \tilde{\mathbf{q}}_e^v - \mathbf{K}_{d\tau}^r \mathbf{v}_e^r - \mathbf{F}_g m \quad (44)$$

where $\tilde{\mathbf{q}}_e^v \in \mathbb{R}^{3 \times 1}$, $\mathbf{F}_g = [-F_g \ 0 \ 0]^T$ is the gravity vector, and the dual part velocity $\mathbf{v}_e^r \in \mathbb{R}^{3 \times 1}$ is the virtual dual error velocity $\dot{\tilde{\mathbf{q}}}_e^v$ for

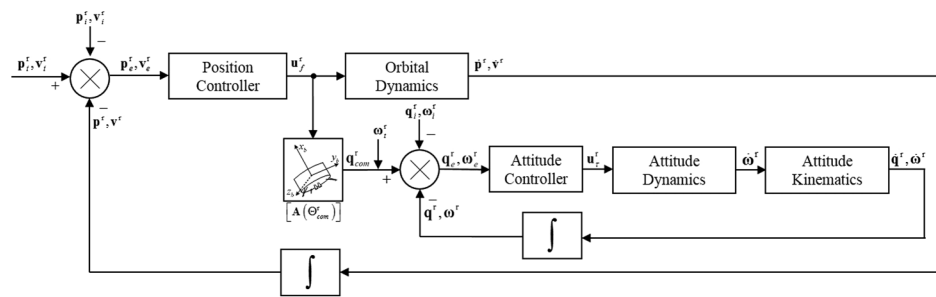


Fig. 4 Lunar landing force-torque sequential control system architecture.

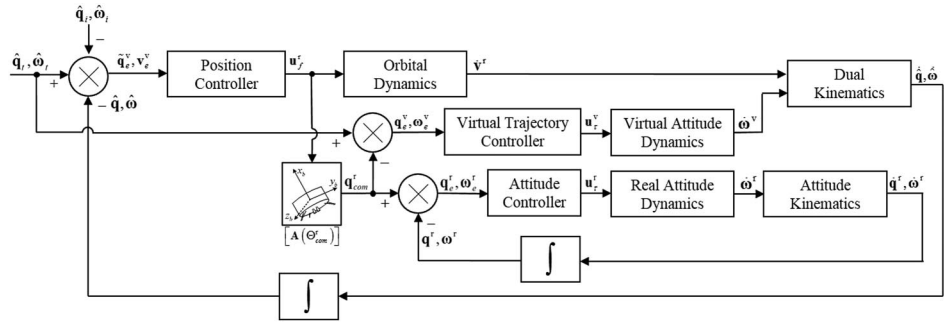
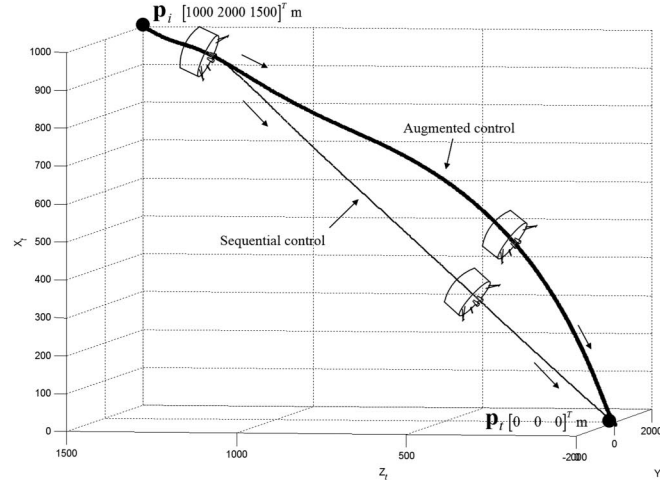


Fig. 5 Virtual trajectory augmented lunar landing control system architecture.

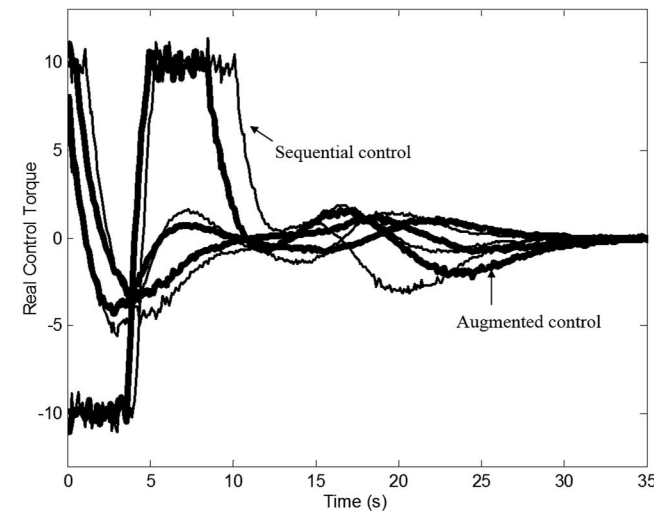
the target velocity. $K_{pf}^r = \text{diag}[K_{pf1}^r, K_{pf2}^r, K_{pf3}^r]$ and $K_{df}^r = \text{diag}[K_{df1}^r, K_{df2}^r, K_{df3}^r]$ are control gains. Equation (44) is considered to be the main contribution of this paper, for which the dual part error of dual quaternion is used as the position error with the variable gain. Herein, DCM $[A(\mathbf{q}^v)]$ for attitude transformation in space can be expressed as

$$[A(\mathbf{q}^v)] = (q_4^{v2} - q^v)^2 \mathbf{1} + 2\mathbf{q}^v\mathbf{q}^{vT} - 2q_4^v[Q^v] \quad (45)$$

where



a) Lander landing trajectories in 3-dimensional space by two control systems, Secs. V.A and V.B

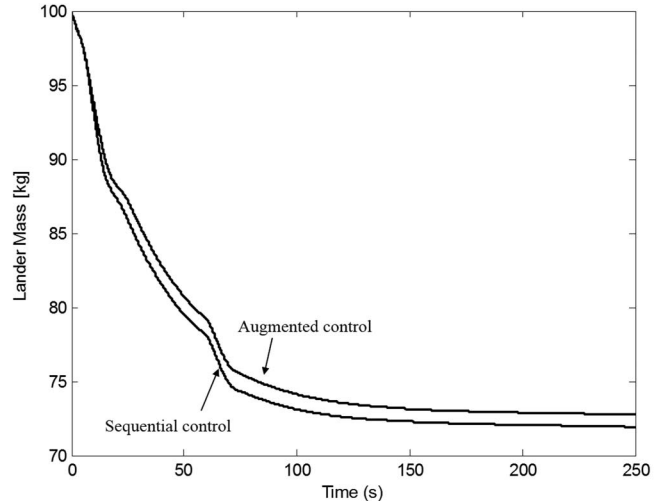


c) Comparison of real control torque between two control systems, Secs. V.A and V.B

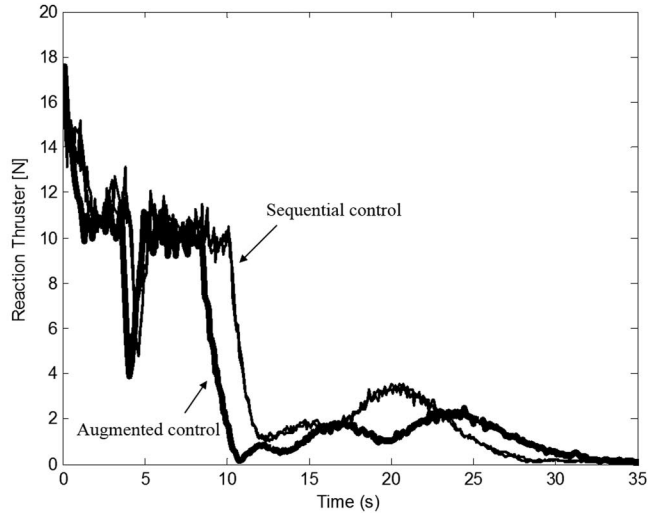
$$Q^v = \begin{bmatrix} 0 & -q_3^v & q_2^v \\ q_3^v & 0 & -q_1^v \\ -q_2^v & q_1^v & 0 \end{bmatrix} \quad (46)$$

C. Virtual Trajectory Augmented Landing Control

The proposed lunar landing controller is sequentially combined with 1) the landing position controller, 2) the lander attitude controller, and 3) the virtual trajectory controller introduced in this



b) Comparison of fuel consumption between two control systems, Secs. V.A and V.B



d) Comparison of real reaction thruster between two control systems, Secs. V.A and V.B

Fig. 6 Comparison between sequential control system and augmented control system.

section. The state variable set X is $[\hat{\omega} \quad \hat{q} \quad \omega^r \quad q^r]$. The dual quaternion \hat{q} and dual angular velocity $\hat{\omega}$ contain the information for the lander's translation and the descent-path angle by multiplication with the lander's position p^r and the lander's velocity v^r and the trajectory variables q^v and ω^v .

The process for the lunar lander's landing control using virtual dual quaternion is summarized in Fig. 5. (For the stability proof, see Appendix A.) First, we set the desired landing angle with the trajectory variable q^v and acquire the dual part \hat{q}_e^v of the dual virtual quaternion error \hat{q}_e^v . We then compute the control force u_f^r with the dual part \hat{q}_e^v as the lander's position error obtained from the multiplication of the real position error p_e^r and virtual quaternion error q_e^v . Herein, there is the key idea that the virtual trajectory error is acquired from the consideration with the real quaternion command q_{com}^r . The target values for the lander's attitude are not to be set. Translational control force vectors are to be set as attitude commands. The descent path for the desired landing angle is made by the rotational controller using the virtual quaternion. The lander translational kinematics then need to be integrated based on the dual quaternion form with the landing path angle information [42].

VI. Simulations and Results

For validation of the proposed approach, some different simulations and results are shown in this section. The first simulation is to compare two control systems, introduced as lunar landing sequential controller (Sec. V.A) and virtual trajectory augmented landing control (Sec. V.C). Figure 6 shows a comparison between the two preceding controllers for the soft landing on the desired landing site. During the terminal landing phase, some cases may occur where the current landing site is no longer desirable. Figure 7 presents an example of retargeting the landing site with the comparison results by two controllers. The third simulation is to analyze several significant parameters for the lander's landing, given in Fig. 8. The fourth simulation is to verify the accuracy of the lander's capability of arriving to a designated position and descending vertically at the desired target position regardless of the difference in the initial velocity when it departs. Results of the simulation are shown in Fig. 9. Table 1 shows the initial conditions of the lunar lander, such as the position, velocity, attitude, and angular velocity, including other main parameters for the simulations. The mass of the lander is assumed as 100 kg, and the inertia matrix of the lander is given as

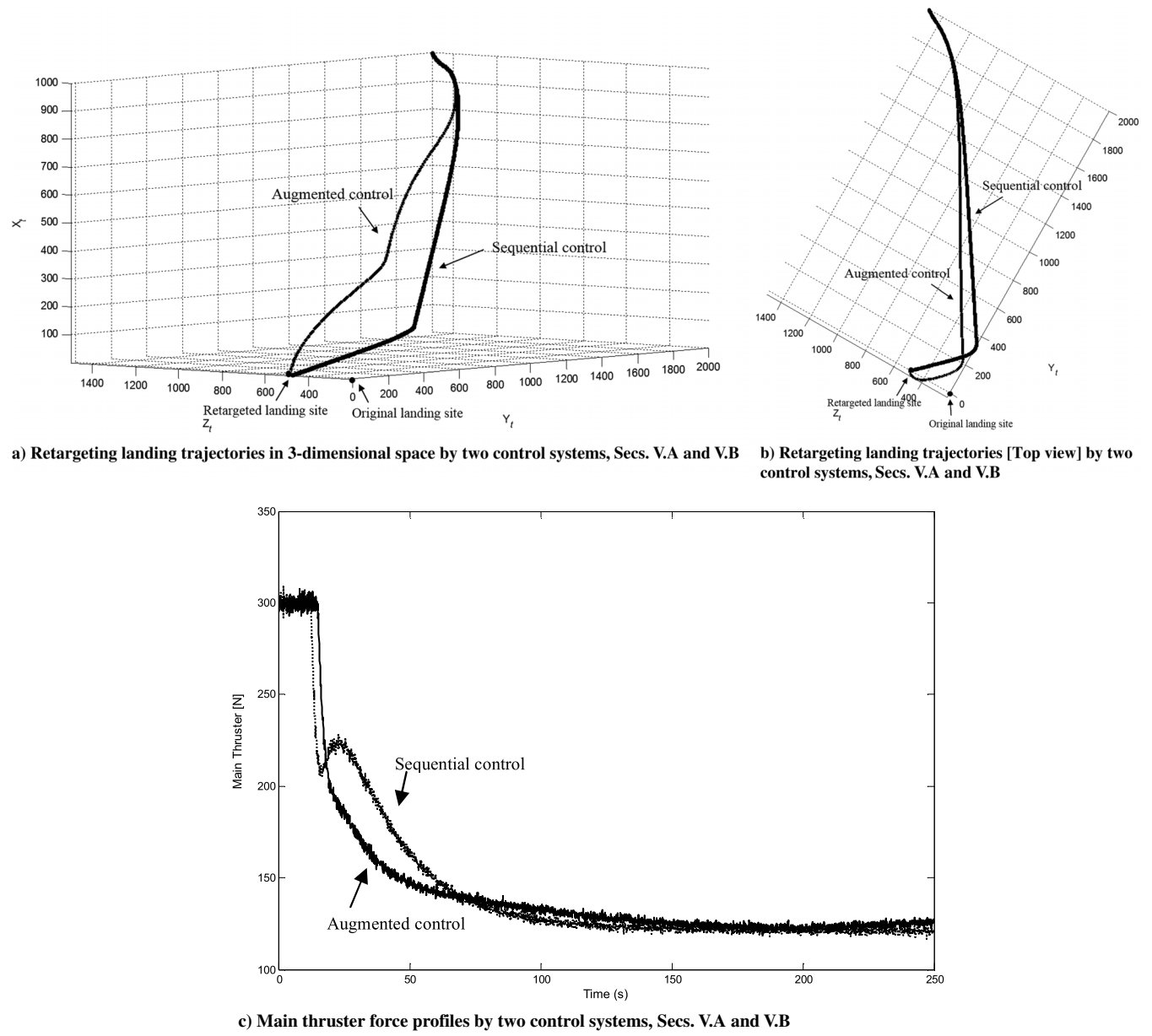
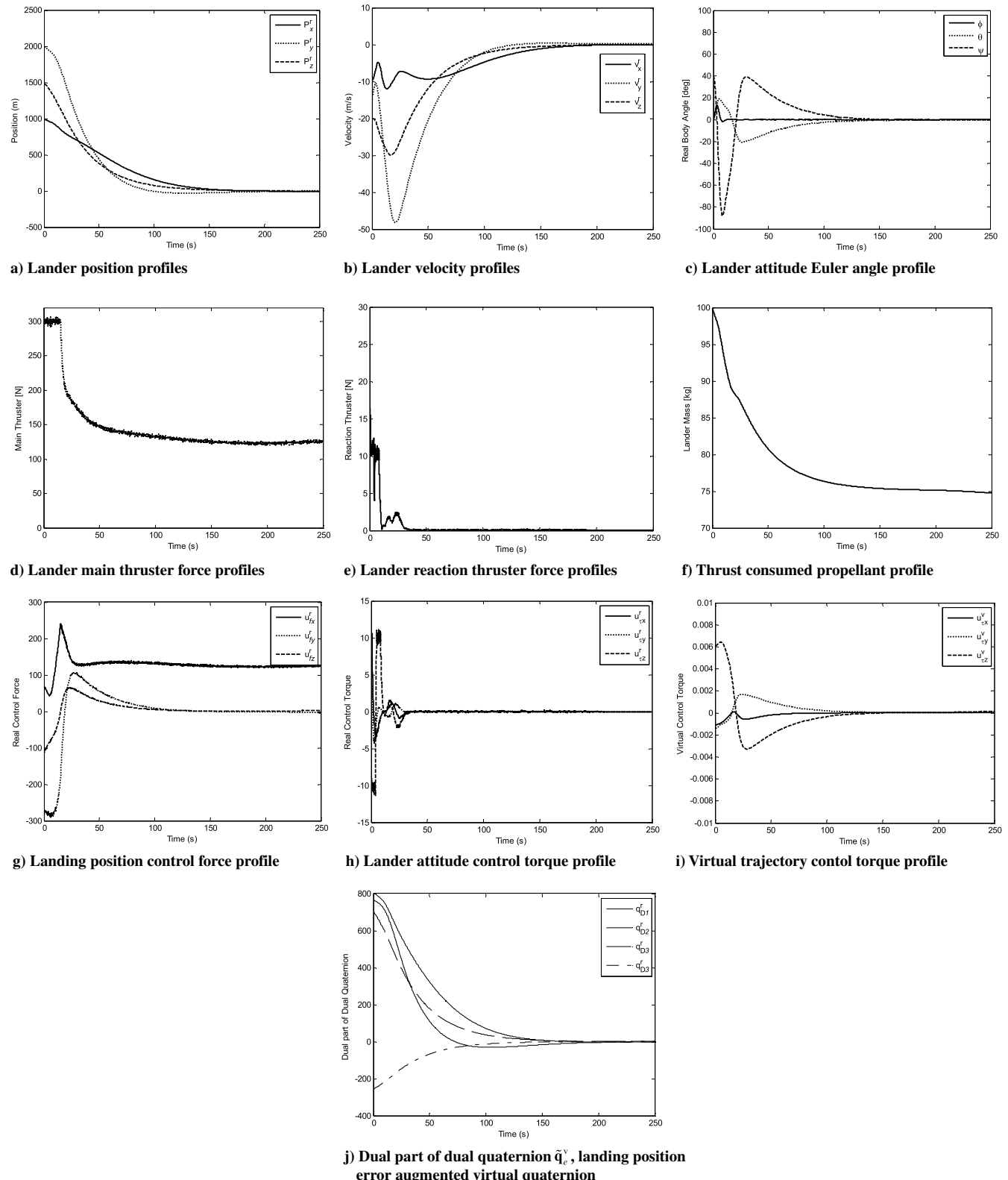


Fig. 7 Comparison of retargeting trajectories between sequential control and augmented control system.

**Fig. 8** Results of landing profiles by augmented control system.

$I = \text{diag}[100, 80, 80] \text{ kg} \cdot \text{m}^2$; other parameters are $\mu = 4902.75 \text{ km}^3/\text{s}^2$, $R_{OT} = 1738 \text{ km}$, and $I_{sp} = 234 \text{ s}$, respectively. The proposed control algorithm is investigated using a Monte Carlo analysis to prove its robustness to deal with the measurement error resulting from sensors and force and reaction thrusters. The measurement error δx is deemed to contain stationary error δx_n and nonstationary scale error δx_s , with the form $\delta x = \delta x_n + \delta x_s$, where δx_n and δx_n are both Gaussian white noises, and corresponding dispersions are set as shown in Table 2. The results of the Monte Carlo

analysis are presented with the retargeting mission in Fig. 10. The controller gains are set as given in Table 3.

The first simulation shows the results of the main parameters, when the lander is slightly moving downward to the target position with small velocities on all three axes: x_t , y_t , and z_t .

This section provides a numerical simulation of a terminal descent mission to demonstrate the effectiveness of the proposed integrated translational and rotational landing strategy. The results of Fig. 6 show that the proposed control law based on the virtual dual

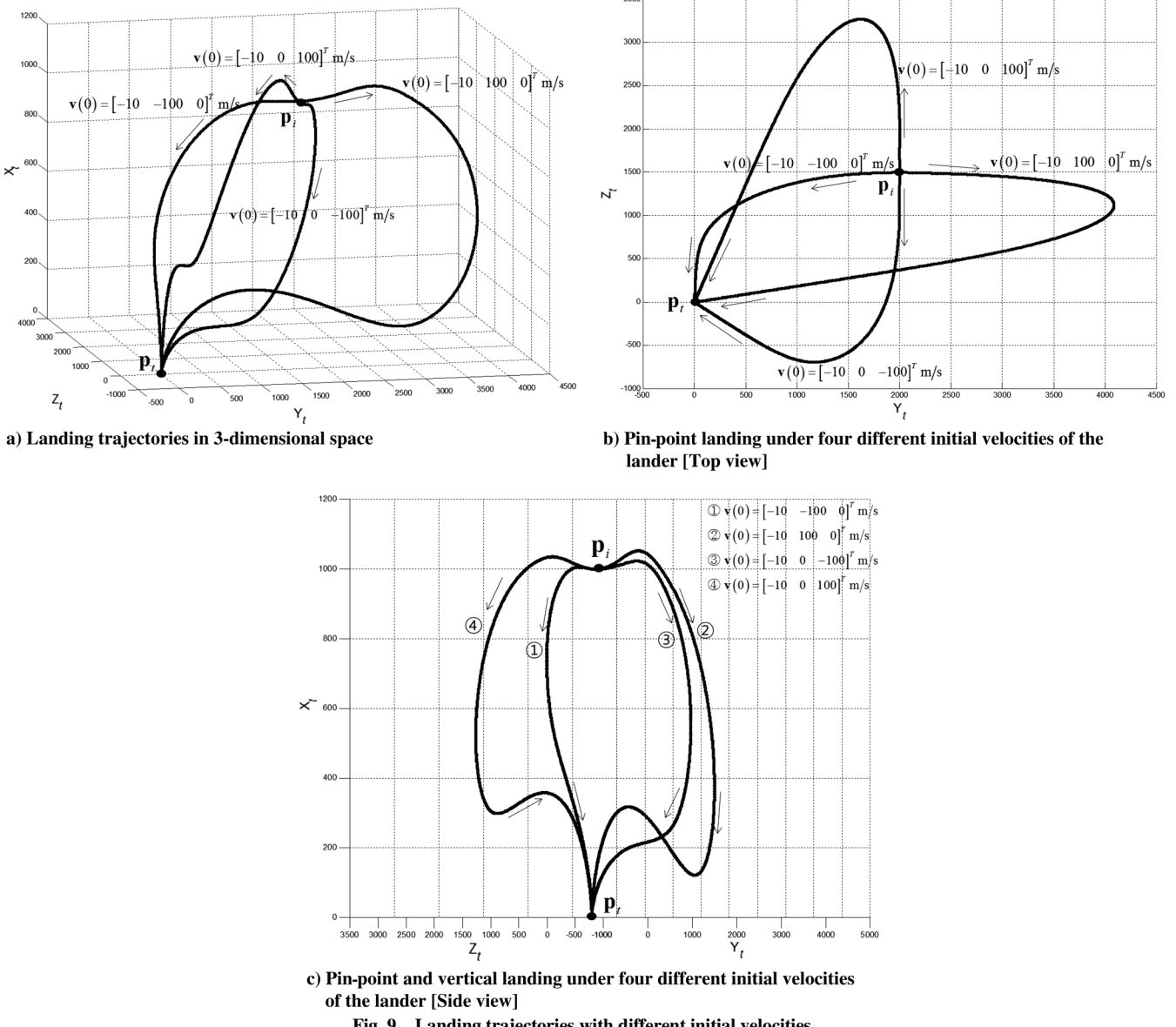


Fig. 9 Landing trajectories with different initial velocities.

quaternion delivered the trajectory by the rotation angle that determines \mathbf{q}^v of $\hat{\mathbf{q}} = \mathbf{q}^v + \epsilon \frac{1}{2} \mathbf{p}^r \circ \mathbf{q}^v$. The result of the sequential control system shows a straight descent because the lander's attitude is controlled by directly targeting the lander's control force vector, whereas the proposed augmented control system enables a smoothly curved soft landing by dual kinematics that combines the real

position and virtual attitude. Dual quaternion assists the lander to descend with smaller attitude control torque, as seen in Figs. 6c and 6d. Figure 7 shows that the proposed control system can provide soft turning to the retargeted landing site. Moreover, the propellant profile shows that the proposed control system consumed less fuel than the force-torque sequential control method. The lander's real significant

Table 1 Initial condition values of simulations

Parameter	Value
Position	$\mathbf{p}^r(t_0) = [1000 \ 2000 \ 1500]^T \text{ m}$ Original landing site: $\mathbf{p}^r(t_f) = [0 \ 0 \ 0]^T \text{ m}$ Retargeted landing site: $\mathbf{p}^r(t_f) = [0 \ 0 \ 500]^T \text{ m}$
Attitude	$\Theta^r(t_0) = [0 \deg \ 0 \deg \ 40 \deg]^T$, $\Theta^r(t_f) = [0 \deg \ 0 \deg \ 0 \deg]^T$
Velocity	$\mathbf{v}^r(t_0) = [-10 \ -15 \ -20]^T \text{ m/s}$ $\mathbf{v}^r(t_0) = [-10 \ -100 \ 0]^T \text{ m/s}$ $\mathbf{v}^r(t_0) = [-10 \ 0 \ -100]^T \text{ m/s}$ $\mathbf{v}^r(t_0) = [-10 \ 100 \ 0]^T \text{ m/s}$ $\mathbf{v}^r(t_0) = [-10 \ 0 \ -100]^T \text{ m/s}$ $\mathbf{v}^r(t_f) = [0 \ 0 \ 0]^T \text{ m/s}$
Angular velocity	$\omega^r(t_0) = [0 \ 0 \ 0]^T \text{ rad/s}$, $\omega^r(t_f) = [0 \ 0 \ 0]^T \text{ rad/s}$
Landing angle	$\rho_t = [0 \deg \ 0 \deg \ 0 \deg]^T$
Maximum descent thrust force	300 N
Maximum reaction thrust force	10 N

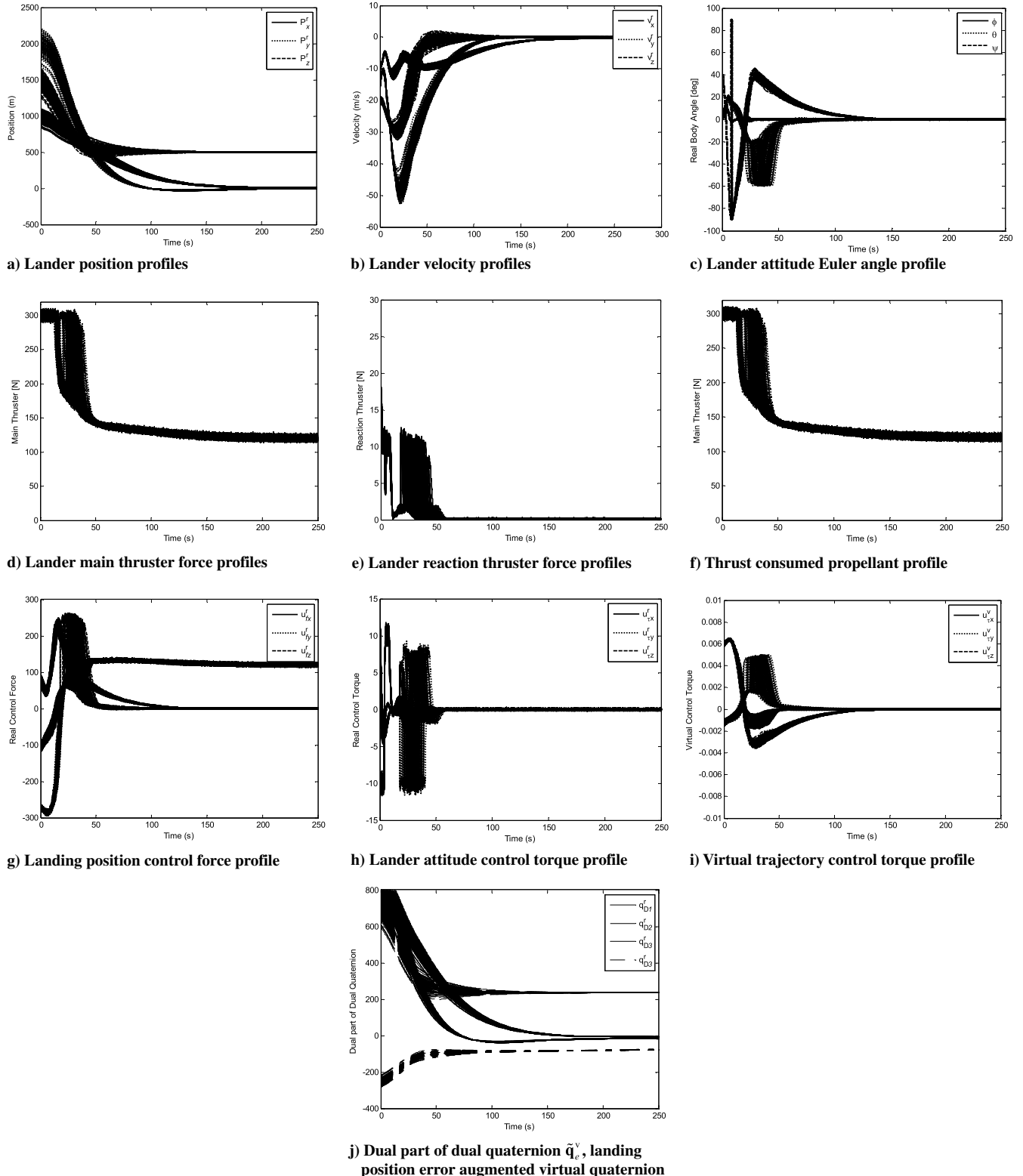


Fig. 10 Results of retargeted landing profiles by augmented control system.

states of Fig. 8 show that the lander can reach the desired target position with the controlled lander's attitude. Furthermore, when the lander arrives at the target position, the attitude of the lander is well controlled such that it is already aligned onto the target frame in Fig. 8c. In the case shown in Figs. 9a–9c, four different initial velocities at initial position \mathbf{p}_i drive the lander's movement along four different virtual trajectories commanded by the virtual quaternion and pinpoint landing at the target position after vertical descent by the desired landing angle $\rho_t = [0 \ 0 \ 0]^T$. Then, according to the

Monte Carlo method, 150 iterations of the numerical simulation are undertaken against the retargeting case. The retargeting missions were successfully performed under the proposed algorithm, as shown in Fig. 10. The descent path with vertical landing angles is set on the proposed controller. From the results of the simulation, the proposed augmented control system is verified to be able to control the landing trajectory by the support as the role of variable gain into the control force. This is caused by the dual quaternion. The attitude of the lunar lander produces smooth pitch-up maneuvering because the attitude

Table 2 Measurement error dispersions

Error	Dispersion	
	Mean (unit)	$3 - \sigma$
$(\delta p^r)_n$, m	0	1
$(\delta v^r)_n$, m/s	0	0.01
$(\delta \Theta^r)_n$, rad	0	0.1
$(\delta \omega^r)_n$, rad/s	0	0.01
$(\delta u^r)_n$, (δu^r_τ) _n , N	0	0
$(\delta p^r)_s$, %	0	2
$(\delta v^r)_s$, %	0	2
$(\delta \Theta^r)_s$, %	0	2
$(\delta \omega^r)_s$, %	0	2
$(\delta u^r)_s$, (δu^r_τ) _s , %	0	5

Table 3 Controller gains set of two simulations

Case	u^r_τ	u^r_f	u^v
$K_p = \omega_n^2 I$	0.1	0.1	0.1
$K_d = 2\xi\omega_n I$	0.9	0.9	0.5

command follows the vector of the control force for the position errors on the descent path. Additionally, the lander reaches the desired target position with a vertical angle to the moon surface, which can be expressed as a pinpoint vertical landing. Therefore, we have demonstrated that the proposed control algorithm can make the lander descend at the required position with a vertical soft landing even on retargeting missions or under different initial velocities of the lunar lander.

VII. Conclusions

This paper presents a new landing technique for a lunar lander. In particular, the terminal landing phase has been analyzed, for which the lunar lander descends with a low speed for touchdown and the attitude controlled to make the lunar lander's attitude vertical with respect to the surface of the moon. The translational dynamics and the rotational dynamics of the lunar lander are mutually coupled when a lunar lander descends, and a sequential control law design of the thrust vector control and attitude control was developed. The proposed control law is able to simultaneously control both the translational position and the rotational attitude. Moreover, the force-torque sequential control law was advanced with the augmentation of kinematics of the dual quaternion to further improve the coupling motion. A new control law is designed based on the virtual dual quaternion as the position error. It was proved that the lunar lander descends along the trajectory formed by the dual part of the virtual dual quaternion. Moreover, dual-quaternion-based dual kinematics that combines real position and virtual attitude assists the lander to descend with small attitude maneuvers. The designed virtual trajectory with the partial guidance was augmented as a direction command into the whole control loop. Simulation results show that the lander's safe landing trajectory control using dual quaternions led to a reduction of the consumed fuel with a vertical descent at the desired target or retargeted landing site, while the attitude of the lander pitches up, preparing the lander to reach the moon surface for terminal touchdown.

To summarize the main proposal, to solve the dynamic coupled problem of a lunar lander, the virtual attitude dynamics and virtual attitude control were additionally considered. The virtual attitude states multiplied with the real position states are used to control the firing vectors of the lander for the ideal landing trajectory, and the controlled firing vectors are regarded as the virtual trajectory. Therefore, as the lander descends along the virtual trajectory, it was verified that the augmented control system improves the dynamic coupled motion and reduces the energy to attain the goal. The new

landing control algorithm could be a solution for future lunar missions with demanding landing performance.

Appendix A: Proof of Stability

A1. Virtual Quaternion Control (Descent-Path Direction)

First, we consider the control of the descent path to be augmented into the translational motion of the lander. From Eq. (A1), it can be shown that $V(\mathbf{q}_e^v, \boldsymbol{\omega}^v)$ is a valid candidate Lyapunov function because $V(\mathbf{q}_e^v = 1, \boldsymbol{\omega}^v = 0) = 0$ and $V(\mathbf{q}_e^v, \boldsymbol{\omega}^v) > 0$ for $(\mathbf{q}_e^v, \boldsymbol{\omega}^v)$, where $\mathbf{q}_e^v = [q_{e1}^v, q_{e2}^v, q_{e3}^v]^T$:

$$\begin{aligned} V(\mathbf{q}_e^v, \boldsymbol{\omega}^v) &= \mathbf{K}_{pt}^v[(q_4^v - 1)^2 + \mathbf{q}^{vT} \mathbf{q}^v] + \frac{1}{2} \boldsymbol{\omega}^{vT} \mathbf{I} \boldsymbol{\omega}^v \\ &= 2\mathbf{K}_{pt}^v(1 - q_4^v) + \frac{1}{2} \boldsymbol{\omega}^{vT} \mathbf{I} \boldsymbol{\omega}^v \end{aligned} \quad (\text{A1})$$

The time derivative of $V(\mathbf{q}_e^v, \boldsymbol{\omega}^v)$ in Eq. (A1) is given by

$$\begin{aligned} \dot{V}(\mathbf{q}_e^v, \boldsymbol{\omega}^v) &= -2\mathbf{K}_{pt}^v \dot{q}_4^v + \boldsymbol{\omega}^{vT} \mathbf{I} \dot{\boldsymbol{\omega}}^v \\ &= \boldsymbol{\omega}^{vT} (\mathbf{K}_{pt}^v \mathbf{q}^v + \mathbf{u}_t^v) \end{aligned} \quad (\text{A2})$$

Note that

$$\dot{\mathbf{q}} = \frac{1}{2} \boldsymbol{\omega}^x \mathbf{q} + \frac{1}{2} q_4 \boldsymbol{\omega}, \quad \dot{q}_4 = -\frac{1}{2} \boldsymbol{\omega}^T \mathbf{q}, \quad \dot{\boldsymbol{\omega}} = \frac{1}{2} \boldsymbol{\omega}^x \mathbf{q} + \frac{1}{2} q_4 \boldsymbol{\omega}$$

With the virtual controller Eq. (41), where \mathbf{K}_{pt}^v and \mathbf{K}_{dt}^v are positive scalars, $\dot{V}(\mathbf{q}_e^v, \boldsymbol{\omega}^v)$ can be made negative semidefinite:

$$\dot{V}(\mathbf{q}_e^v, \boldsymbol{\omega}^v) = -\mathbf{K}_{dt}^v \boldsymbol{\omega}^{vT} \boldsymbol{\omega}^v \leq 0 \quad (\text{A3})$$

Because $V(\mathbf{q}_e^v, \boldsymbol{\omega}^v)$ is continuously differentiable, radially unbounded, positive-definite, and $\dot{V}(\mathbf{q}_e^v, \boldsymbol{\omega}^v) \leq 0$ over the entire state space, by using LaSalle's invariance principle, all descent paths must converge to the invariant set in $\{(\mathbf{q}_e^v, \boldsymbol{\omega}^v) : \dot{V} = 0\} = \{(\mathbf{q}_e^v, \boldsymbol{\omega}^v) : \boldsymbol{\omega}^v = 0\}$ [43,44].

A2. Position Control of Lander

Second, we discuss the stability of the translational control Eq. (44) of the lander. Substituting Eq. (44) into Eq. (22), we obtain

$$\dot{\mathbf{v}}^r = \mathbf{K}_{pf}^r \tilde{\mathbf{q}}_e^v + \mathbf{K}_{df}^r \mathbf{v}_e^r \quad (\text{A4})$$

Equation (A4) can be rewritten as

$$\ddot{\mathbf{p}}_e^r - \mathbf{K}_{df}^r \dot{\mathbf{p}}_e^r - \mathbf{K}_{pf}^r \tilde{\mathbf{q}}_e^v = 0 \quad \ddot{\mathbf{p}}_e^r - \mathbf{K}_{df}^r \dot{\mathbf{p}}_e^r - \mathbf{K}_{pf}^r \frac{1}{2} (\mathbf{p}_e^r \circ \mathbf{q}_e^v) = 0 \quad (\text{A5})$$

$\tilde{\mathbf{q}}_e^v$ denotes the dual part of the virtual dual error quaternion $\hat{\mathbf{q}}_e^v$ in Eq. (43). \mathbf{q}_e^v of third term of Eq. (A5) that is multiplied with \mathbf{p}_e^r is verified to be converged to the equilibrium point $\mathbf{q}_e^v(t) = (0, 0, 0, 1)$, if $t \rightarrow \infty$ by the given Eqs. (A1–A3). Therefore, if both control gains \mathbf{K}_{pf}^r and \mathbf{K}_{df}^r of Eq. (A5) are chosen as positive values so that the characteristic roots of Eq. (A5) have negative real parts, \mathbf{p}_e^r then approaches zero asymptotically as well as \mathbf{v}^r and $\dot{\mathbf{v}}^r$. Synthesizing the discussions about the stability of $\tilde{\mathbf{q}}_e^v$ in Eq. (A4) is the dual part of $\hat{\mathbf{q}}_e^v$ in Eq. (43), when $t \rightarrow \infty$, $\hat{\mathbf{q}}_e^v(\tilde{\mathbf{q}}_e^v) = \mathbf{q}_e^v(t) + \epsilon \frac{1}{2} (\mathbf{p}_e^r(t) \circ \mathbf{q}_e^v(t))$ will asymptotically converge to $\hat{\mathbf{q}}_e^v(t) = (0, 0, 0, 0) + \epsilon(0, 0, 0, 0)$.

A3. Attitude Control of Lander

For attitude control of the lander, the proof of the stability is similar to that of virtual quaternion control for the descent path. From Eq. (A6), it can be shown that $V(\mathbf{q}_e^r, \boldsymbol{\omega}^r)$ is a valid candidate

Lyapunov function because $V(\mathbf{q}_e^r = 1, \boldsymbol{\omega}^r = 0) = 0$ and $V(\mathbf{q}_e^r, \boldsymbol{\omega}^r) > 0$ for $(\mathbf{q}_e^r, \boldsymbol{\omega}^r)$, where $\mathbf{q}_e^r = [q_{e1}^r, q_{e2}^r, q_{e3}^r]^T$:

$$\begin{aligned} V(\mathbf{q}_e^r, \boldsymbol{\omega}^r) &= \mathbf{K}_{pr}^r[(q_4^r - 1)^2 + \mathbf{q}^{rT} \mathbf{q}^r] + \frac{1}{2} \boldsymbol{\omega}^{rT} \mathbf{I} \boldsymbol{\omega}^r \\ &= 2\mathbf{K}_{pr}^r(1 - q_4^r) + \frac{1}{2} \boldsymbol{\omega}^{rT} \mathbf{I} \boldsymbol{\omega}^r \end{aligned} \quad (\text{A6})$$

The time derivative of $V(\mathbf{q}_e^r, \boldsymbol{\omega}^r)$ in Eq. (A6) is given by

$$\dot{V}(\mathbf{q}_e^r, \boldsymbol{\omega}^r) = -2\mathbf{K}_{pr}^r q_4^r + \boldsymbol{\omega}^{rT} \mathbf{I} \dot{\boldsymbol{\omega}}^r = \boldsymbol{\omega}^{rT} (\mathbf{K}_{pr}^r \mathbf{q}^r + \mathbf{u}_r^r) \quad (\text{A7})$$

With the attitude controller Eq. (39), where \mathbf{K}_{pr}^r and \mathbf{K}_{dt}^r are positive scalars, $\dot{V}(\mathbf{q}_e^r, \boldsymbol{\omega}^r)$ can be made negative semidefinite:

$$\dot{V}(\mathbf{q}_e^r, \boldsymbol{\omega}^r) = -\mathbf{K}_{dt}^r \boldsymbol{\omega}^{rT} \boldsymbol{\omega}^r \leq 0 \quad (\text{A8})$$

Because $V(\mathbf{q}_e^r, \boldsymbol{\omega}^r)$ is continuously differentiable, radially unbounded, positive-definite, and $\dot{V}(\mathbf{q}_e^r, \boldsymbol{\omega}^r) \leq 0$ over the entire state space, by using LaSalle's invariance principle, all descent paths must converge to the invariant set in $\{(\mathbf{q}_e^r, \boldsymbol{\omega}^r) : \dot{V} = 0\} = \{(\mathbf{q}_e^r, \boldsymbol{\omega}^r) : \boldsymbol{\omega}^r = 0\}$ [43,44].

References

- [1] Cherry, G., "A General Explicit, Optimizing Guidance Law for Rocket-Propelled Spaceflight," *AIAA Astrodynamics Guidance and Control Conference*, AIAA Paper 1964-0638, 1964.
- [2] Klumpp, A. R., "Apollo Guidance Navigation Control," Charles Stark Draper Lab. Rept. R-695, Cambridge, MA, June 1971.
- [3] Klumpp, A. R., "Apollo Lunar Descent Guidance," *Automatica*, Vol. 10, No. 2, 1974, pp. 133–146.
doi:10.1016/0005-1098(74)90019-3
- [4] Kriegsman, B. A., and Reiss, M. H., "Terminal Guidance and Control Techniques for Soft Lunar Landing," *ARS Journal*, Vol. 32, No. 3, 1962, pp. 401–413.
- [5] Uena, S., and Yamaguchi, Y., "3-Dimensional Near-Minimum Fuel Guidance Law of a Lunar Landing Module," *AIAA Guidance, Navigation, and Control Conference and Exhibit*, AIAA Paper 1999-3983, 1999.
- [6] Afshari, H. H., and Novinzadeh, A., "A Perturbation Approach in Determination of Closed-Loop Optimal-Fuzzy Control Policy for Planetary Landing Mission," *Proceedings of the Institution of Mechanical Engineers, Part G: Journal of Aerospace Engineering*, Vol. 223, No. 3, 2009, pp. 233–243.
doi:10.1243/09544100JAERO429
- [7] Cheng, R. K., and Conrad, D. A., "Design Considerations for the Surveyor Terminal Descent System," *AIAA/ION Astrodynamics Guidance and Control Conference*, AIAA Paper 1964-644, Aug. 1964.
- [8] Ramanan, R., and Lal, M., "Analysis of Optimal Strategies for Soft Landing on the Moon from Lunar Parking Orbits," *Journal of Earth System Science*, Vol. 114, No. 6, 2005, pp. 807–813.
doi:10.1007/BF02715967
- [9] Bei, C., and Zhang, W., "A Guidance and Control Solution for Small Lunar Probe Precise Landing Mission," *Acta Astronautica*, Vol. 62, No. 1, 2008, pp. 44–47.
doi:10.1016/j.actaastro.2006.12.047
- [10] Li, M., Macdonald, M., McInnes, C., and Jing, W., "Analytical Landing Trajectories for Embedded Autonomy," *Proceedings of the Institution of Mechanical Engineers, Part G: Journal of Aerospace Engineering*, Vol. 224, No. 11, 2010, pp. 1177–1191.
doi:10.1243/09544100JAERO759
- [11] Guo, J., and Han, C., "Design of Guidance Laws for Lunar Pinpoint Soft Landing," *AAS Astrodynamics Conference*, AAS Paper 2009-431, 2009.
doi:10.1243/09544100JAERO429
- [12] Wang, D., Huang, X., and Guan, Y., "GNC System Scheme for Lunar Soft Landing Spacecraft," *Advances in Space Research*, Vol. 42, No. 2, 2008, pp. 379–385.
doi:10.1016/j.asr.2007.08.031
- [13] Citron, S. J., Dunin, S. E., and Meissinger, H. F., "A Terminal Guidance Technique for Lunar Landing," *AIAA Journal*, Vol. 2, No. 3, 1964, pp. 503–509.
doi:10.2514/3.2362
- [14] Jungmann, A., "Gravity Turn Trajectories Through Planetary Atmospheres," *Control and Flight Dynamics Conference*, AIAA Paper 1967-0596, 1967.
- [15] McInnes, C., "Direct Adaptive Control for Gravity-Turn Descent," *Journal of Guidance, Control, and Dynamics*, Vol. 22, No. 2, 1998, pp. 373–375.
doi:10.2514/2.4392
- [16] McInnes, C., "Gravity-Turn Descent from Low Circular Orbit Conditions," *Journal of Guidance, Control, and Dynamics*, Vol. 26, No. 1, 2003, pp. 183–185.
doi:10.2514/2.5033
- [17] Chomel, C., and Bishop, R., "An Analytical Lunar Descent Guidance Algorithm," *Journal of Guidance, Control, and Dynamics*, Vol. 32, No. 3, 2009, pp. 915–926.
doi:10.2514/1.37700
- [18] Sun, J., Cui, P., and Liu, Q., "Fuzzy Control Application to Guidance Control for Lunar Gravity-Turn," *International Conference on Machine Learning and Cybernetics*, Vol. 9, Aug. 2005, pp. 5635–5640.
doi:10.1109/ICMLC.2005.1527940
- [19] Widnall, W., "Lunar Module Digital Autopilot," *Journal of Spacecraft and Rockets*, Vol. 8, No. 1, 1971, pp. 56–62.
doi:10.2514/3.30217
- [20] Açıkmese, B., and Ploen, S. R., "Convex Programming Approach to Powered Descent Guidance for Mars Landing," *Journal of Guidance, Control, and Dynamics*, Vol. 30, No. 5, Sept.–Oct. 2007, pp. 1353–1366.
doi:10.2514/1.27553
- [21] Chomel, C. T., and Bishop, H. R., "Analytical Lunar Descent Guidance Algorithm," *Journal of Guidance, Control, and Dynamics*, Vol. 32, No. 3, May–June 2009, pp. 915–926.
doi:10.2514/1.37700
- [22] Blackmore, L., Açıkmese, B., and Scharf, D. P., "Minimum-Landing-Error Powered-Descent Guidance for Mars Landing Using Convex Optimization," *Journal of Guidance, Control, and Dynamics*, Vol. 33, No. 4, July–Aug. 2010, pp. 1161–1171.
doi:10.2514/1.47202
- [23] Clifford, W., "Preliminary Sketch of Bi-Quaternions," *Proceedings of the London Mathematical Society*, Vol. 4, No. 1, 1873, pp. 381–395.
- [24] Yang, A. T., and Freudenstein, F., "Application of Dual-Number Quaternion Algebra to the Analysis of Spatial Mechanisms," *Journal of Applied Mechanics*, Vol. 31, No. 2, June 1964, pp. 300–308.
doi:10.1115/1.3629601
- [25] Xu, Y., Hu, X. D., Li, T., and Lian, J., "Strapdown Inertial Navigation System Algorithms Based on Dual Quaternions," *IEEE Transactions on Aerospace and Electronic Systems*, Vol. 41, No. 1, 2004, pp. 110–132.
doi:10.1109/TAES.2005.1413751
- [26] Dong, G., Liao, Q., Wei, S., Dai, J., and Qiao, S., "Dual Quaternion-Based Inverse Kinetics of the General Spatial 7R Mechanism," *Proceedings of the Institution of Mechanical Engineering Science*, Vol. 222, No. 8, 2008, pp. 1593–1598.
doi:10.1243/09544062JMES1082
- [27] Wang, J., Liang, H., Sun, Z., Wu, S., and Zhang, S., "Relative Motion Coupled Control Based on Dual Quaternion," *Aerospace Science and Technology*, Vol. 25, No. 1, March 2013, pp. 102–113.
doi:10.1016/j.ast.2011.12.013
- [28] Zhang, F., and Duan, G., "Robust Integrated Translation and Rotation Finite-Time Maneuver of a Rigid Spacecraft Based on Dual Quaternion," *AIAA Guidance, Navigation, and Control Conference*, AIAA Paper 2011-6396, Aug. 2011.
doi:10.2514/6.2011-6396
- [29] Perez, A., and McCarthy, J. M., "Dual Quaternion Synthesis of Constrained Robotic Systems," *Journal of Mechanical Design*, Vol. 126, No. 3, 2004, pp. 425–435.
doi:10.1115/1.1737378
- [30] Ge, Q., and Ravani, B., "Computer Aided Geometric Design of Motion Interpolants," *ASME Journal of Mechanical Design*, Vol. 116, No. 3, 1994, pp. 756–762.
doi:10.1115/1.2919447
- [31] Goddard, J., "Pose and Motion Estimation from Vision Using Dual Quaternion Based Extended Kalman Filtering," Ph.D. Thesis, Univ. of Tennessee, Knoxville, TN, 1997.
- [32] Daniilidis, K., "Hand-Eye Calibration Using Dual Quaternions," *International Journal of Robotics Research*, Vol. 18, No. 3, 1999, pp. 286–298.
doi:10.1177/02783649922066213
- [33] Kuipers, J. B., "Quaternions and Rotation Sequences: A Primer with Applications to Orbits," *Aerospace and Virtual Reality*, Princeton Univ. Press, Princeton, NJ, 1999, Chaps. 9, 11.

- [34] van den Bergen, G., "Dual Numbers: Simple Math, Easy C++ Coding, and Lots of Tricks," GDC Europe, 2009, <http://www.gdcvault.com/play/10103/Dual-Numbers-Simple-Math-Easy>.
- [35] Fischer, S., *Dual-Number Methods in Kinematics, Statics and Dynamics*, CRC Press, Boca Raton, FL, 1999, Chap. 3.
- [36] Sabata, B., and Aggarwal, J. K., "Estimation of Motion from a Pair of Range Images: A Review," *CVGIP: Image Understanding*, Vol. 54, No. 3, 1991, pp. 309–324.
doi:10.1016/1049-9660(91)90032-K
- [37] Keler, M. L., "On the Theory of Screws and the Dual Method," *Proceedings of a Symposium Commemorating the Legacy, Works, and Life of Sir Robert Stawell Ball Upon the 100th Anniversary of "A Treatise on the Theory of Screws"*, Univ. of Cambridge, Trinity College, Cambridge, England, U.K., July 2000.
- [38] Wang, X., Han, D., Yu, C., and Zheng, Z., "The Geometric Structure of Unit Dual Quaternion with Application in Kinematic Control," *Journal of Mathematical Analysis and Applications*, Vol. 389, No. 2, May 2012, pp. 1352–1364.
doi:10.1016/j.jmaa.2012.01.016
- [39] Filipe, N., and Tsiotras, P., "Adaptive Position and Attitude-Tracking Controller for Satellite Proximity Operations Using Dual Quaternions," *Journal of Guidance, Control, and Dynamics*, Vol. 38, No. 4, 2015,
pp. 566–577.
doi:10.2514/1.G000054
- [40] Zhang, F., and Duan, G.-R., "Integrated Translational and Rotational Control for the Terminal Landing Phase of a Lunar Module," *Aerospace Science and Technology*, Vol. 27, No. 1, June 2013, pp. 112–126.
doi:10.1016/j.ast.2012.07.003
- [41] Sidi, M. J., *Spacecraft Dynamics and Control: A Practical Engineering Approach*, Cambridge Univ. Press, Cambridge, England, U.K., 1997, pp. 318–327.
- [42] Kwon, J. W., Lee, D., and Bang, H., "Coupled Dynamics Lunar Landing Control Based on Dual Quaternions," *Proceedings of the 3rd CEAS EuroGNC, Specialist Conference on Guidance, Navigation & Control*, ONERA, ISAE-SUPAERO & ENAC, Toulouse, France, April 2015.
- [43] Wie, B., Weiss, H., and Arapostathis, A., "Quaternion Feedback Regulator for Spacecraft Eigenaxis Rotations," *Journal of Guidance*, Vol. 12, No. 3, May–June 1989, pp. 375–380.
doi:10.2514/3.20418
- [44] Lizarralde, F., and Wen, J. T., "Attitude Control Without Angular Velocity Measurement: A Passivity Approach," *IEEE Transactions on Automatic Control*, Vol. 41, No. 3, March 1996.
doi:10.1109/9.486654